



Hydrodeoxygenation of guaiacol over Ni@Pd and Ni@Pt bimetallic overlayer catalysts

Qinghua Lai, Chen Zhang, Joseph H. Holles*

Department of Chemical Engineering, University of Wyoming, Dept. 3295, 1000 E. University Ave, Laramie, WY 82071, United States



ARTICLE INFO

Article history:

Received 7 June 2016

Received in revised form 30 August 2016

Accepted 17 September 2016

Available online 17 September 2016

Keywords:

Guaiacol

Hydrodeoxygenation

Overlayer

Hydrogen chemisorption

Bimetallic

Pd

Pt

ABSTRACT

First principle computational studies have predicted that formation of Pd or Pt overlayer on Ni base metal would cause a negative shift of the d-band center of surface Pd or Pt, resulting in reduced binding strength for adsorbed species. In this paper, silica alumina supported Ni@Pd and Ni@Pt overlayer catalysts were synthesized via directed deposition technique and tested for hydrodeoxygenation of guaiacol at atmospheric pressure. Several characterization techniques such as hydrogen chemisorption, ethylene hydrogenation descriptor reaction, XRD and TEM studies were employed to characterize the catalysts. H₂ chemisorption results showed that Ni@Pd and Ni@Pt overlayer catalysts had reduced H₂ adsorption strength compared to Pd or Pt only catalysts, which agreed with the computational prediction. As predicted, the overlayer catalysts also showed lower activity for ethylene hydrogenation than Pd or Pt only catalysts. XRD and TEM studies indicated that overlayers have been successfully deposited atop supported nickel. Guaiacol hydrodeoxygenation results showed that, especially at low reaction temperature, Pd and Pt active sites of overlayer catalysts showed significantly enhanced deoxygenation activity compared with that of Pd or Pt only catalysts. Further studies showed that guaiacol could be completely deoxygenated using silica alumina supported metal catalysts, yielding benzene, toluene, and xylenes as major products.

© 2016 Elsevier B.V. All rights reserved.

1. Introduction

Currently, the major portion of the global energy supply relies on energy produced from fossil-based resources. One of the major concerns of society today as related to energy is the depletion of petroleum, a non-renewable fossil source of carbon. Another major society concern is the use of fossil fuels resulting in subsequent environmental problems including greenhouse gas emissions and acid rain. Hence, there is a need to switch to clean, renewable sources of energy.

Lignocellulosic biomass is the most abundant class of biomass on the planet [1]. It provides an opportunity to be used as a sustainable source of energy and organic carbon for our society. Lignocellulosic biomass can be converted into crude bio-oil via thermochemical treatment such as pyrolysis or liquefaction. These crude bio-oils are multicomponent mixtures of a large number of oxygenated compounds. However, the high oxygen content of crude bio-oils, usually 20 to 50 wt%, leads to low heating value, poor stability, poor volatility, high viscosity and corrosiveness [2,3]. Therefore, oxygen

removal from bio-oils is necessary for further application as liquid fuels.

The lignin fraction of biomass is a three-dimensional amorphous polymer composed of methoxylated phenylpropane structures, which contains approximately 40% of the possible energy of the biomass [4]. Compared with the carbohydrate fraction of biomass, it is more attractive to derive alternative fuels from the lignin fraction because it has a lower oxygen-to-carbon ratio. There are several approaches for upgrading bio-oils including zeolite upgrading [3,5–8], aqueous phase processing [8,9] and hydrotreating [3–5,9,10]. Hydrotreating, in which feedstocks are reacted with hydrogen in the presence of a catalyst, is the most common method to upgrade bio-oil to hydrocarbons via a hydrodeoxygenation (HDO) reaction to remove oxygen [3,4]. HDO studies of lignin-derived oils usually employ model compounds such as phenols, anisole and guaiacol instead of bio-oil. Guaiacol, which has two types of C–O bonds (C–OH bond and C–OCH₃ bond), appears to be the preferred choice as a prototype compound to represent lignin-derived bio-oils.

The traditional HDS catalysts (sulfided Co-Mo/γ-Al₂O₃ or Ni-Mo/γ-Al₂O₃) used in petroleum refining are also utilized as HDO catalysts [3,11]. However, these conventional hydrodeoxygenation catalysts have some disadvantages such as possible sulfur con-

* Corresponding author.

E-mail address: jholles@uwyo.edu (J.H. Holles).

tamination of products, rapid deactivation by coke formation and water-induced catalyst deactivation [3,11,12]. For these reasons, non-sulfided transition metal based catalysts systems are being developed for the HDO of lignin and related model compounds. HDO of lignin related model compounds by base metal catalysts, such as supported Ni [13–19], Fe [20,21], and Mo [22–25] have been investigated. The supported metal phosphides (Ni_2P , Fe_2P , Co_2P , MoP , WP) were also used as catalysts for HDO of guaiacol and anisole [26–28]. Ni_2P showed the highest activity for HDO among tested metal phosphides (Ni_2P , Co_2P , MoP , WP) [26,27]. Recently, using supported noble metals as effective HDO catalysts has received new attention [29–33]. These noble metal catalysts are generally highly active for hydrogenation and hydrogenolysis, and require lower temperature or pressure than conventional hydrotreating catalysts [3]. However, the noble metal catalysts are expensive and are highly active for hydrogenation of aromatic rings causing high H_2 consumptions.

Using bimetallic catalysts is a strategy to enhance the efficiency of catalysts for HDO, as the interaction between metals can modify the geometric and electronic structures of metal surface resulting in improved catalytic activity and selectivity [3,4,34–37]. In related work, Lobo et al. have reported that adding Ni or Co into the Pt not only increased the meta-cresol HDO activity, but also enhanced formation of methylcyclohexane as well [38]. Resasco et al. have shown that a bimetallic Pt-Sn catalyst used for HDO of guaiacol at high temperatures (400°C) had higher reactivity (80% conversion after 3 h time-on-stream) and better stability than the monometallic catalyst [39]. They postulated that the strong adsorption of double-functionalized guaiacol (or catechol) on the catalyst surface could block sites for deoxygenation on the Pt catalyst, and the bimetallic Pt-Sn might be able to reduce the binding strength. Ardiyanti et al. investigated HDO of anisole over $\text{Ni}-\text{Cu}/\delta-\text{Al}_2\text{O}_3$ with various Ni/Cu ratios [40]. The bimetallic Ni–Cu catalyst showed higher activity than monometallic nickel, which may be attributed to more formation of active metallic nickel when the copper is present. Wang et al. also have found that the bimetallic Pd-Fe/C catalyst exhibit a substantially enhanced activity of HDO of guaiacol, with more than 80% yield to benzene/toluene/trimethylbenzene at 450°C [41]. The single crystal studies of Ni/Pt overlayer system by Chen et al. have shown a bimetallic Ni/Pt surface binds hydrogen and unsaturated hydrocarbon adsorbates more weakly than corresponding monometallic surfaces and thus enhanced the activity toward the production of butene in HDS of thiophene [42]. The formation of weaker metal-adsorbate bonds was speculated to be favorable to overcome the kinetic barrier for the HDS of thiophene.

Based on previous literature work using bimetallic catalysts for HDO, the pseudomorphic overlayer catalyst with a monolayer of metal atop a base metal would also enhance HDO activity. Studies have shown that adsorbate bond strengths are generally altered in overlayer systems due to the shift of the d-band center of the overlaying metal [43–47]. Our previous research demonstrated that pseudomorphic overlayer catalysts, such as Ni@Pt, Co@Pt or Re@Pd (core@shell), could reduce H_2 and CO binding energy when compared to single metal and alloy counterparts, as predicted from computational work [48–51]. The decrease in hydrogen and hydrocarbon adsorbates binding strength indicate that pseudomorphic overlayer catalysts may demonstrate improved performance for the HDO reaction because strong bonding has been shown to inhibit the reaction [39]. Ni@Pd and Ni@Pt overlayers have been predicted to have negative d-band shifts and decreased binding strength compared to the pure Pd or Pt [43–46]. In this contribution, we synthesized single deposition Ni@Pd and Ni@Pt overlayer catalysts and used a strategy of reducing binding strength to improve the efficiency of catalysts for guaiacol HDO. H_2 chemisorption, ethylene hydrogenation descriptor reaction, physical sorption, XRD and

TEM studies were conducted to characterize the catalysts. Guaiacol HDO reactivity tests were performed in a fixed-bed reactor at atmospheric pressure to study how overlayer catalysts affect HDO activity.

2. Experimental

2.1. Preparation of catalysts

The monometallic Ni, Pd and Pt catalysts and non-structured bimetallic catalysts were prepared using co-impregnation method. A silica-alumina catalyst support (Alfa Aesar, grade 135) was used as support for all catalysts. The precursors used in this paper were nickel nitrate hexahydrate (Aldrich 99.999%), palladium (II) acetylacetone (Alfa Aesar) and platinum (II) acetylacetone (Alfa Aesar). The metal loading was about 0.5 wt% for monometallic Pt and Pd catalysts, and 5 wt% for Ni parent catalysts. The non-structured bimetallic Ni–Pd and Ni–Pt catalysts were prepared with similar metal loadings as the overlayer catalysts. After impregnation of silica-alumina with a solution of precursors (aqueous solution for nickel nitrate hexahydrate and toluene solution for palladium (II) acetylacetone and platinum (II) acetylacetone), the mixtures were heated at around 60°C to evaporate solvent. All mixtures were dried in an oven overnight. For bimetallic catalysts, the nickel nitrate hexahydrate was impregnated first and then the dry mixture was used for the second impregnation to load Pd or Pt. Then the dry catalysts were calcined in air at 400°C for 3 h using a $3^\circ\text{C}/\text{min}$ ramp rate [52,53]. The catalysts were then reduced under 60 sccm H_2 flow at 450°C for 3 h using a $3^\circ\text{C}/\text{min}$ ramp rate based on suggestions in the literature [50,52–55].

The overlayer catalysts used in this paper were synthesized using the directed deposition method [49,50]. Typically, the parent $\text{Ni/SiO}_2-\text{Al}_2\text{O}_3$ catalyst was reduced in 60 sccm H_2 flow at 450°C for 4 h using a $3^\circ\text{C}/\text{min}$ ramp rate. Then water-saturated helium gas was passed over the catalyst for 24 h at room temperature. After that, the parent catalyst was treated with 60 sccm H_2 flow at 60°C for 1 h (to maximize H_2 adsorption for the subsequent overlayer deposition reaction). The briefly reduced sample was directly poured from reduction reactor into a toluene solution (30 mL) of 0.1 M acetylacetone, with H_2 gas flowing into the reduction reactor at same time. Acetylacetone was used as a surface inhibitor to minimize the platinum adsorption on the support. After 15 min surface deactivation, a toluene solution of 0.05 M Pd (II) acetylacetone (or Pt (II) acetylacetone) was added. The mixture was then kept at 60°C for 2 h. The amount of Pd (II) acetylacetone added was equivalent to the 150% monolayer coverage of parent Ni surface. The catalyst was then vacuum filtered and placed in a 110°C oven overnight. The dried catalyst was calcined in near stagnant air at 400°C for 4 h using a $3^\circ\text{C}/\text{min}$ ramp rate. After calcination, the catalyst was reduced in H_2 flow at calcine temperatures for 4 h using a $3^\circ\text{C}/\text{min}$ ramp rate.

2.2. Catalyst characterization

Inductively coupled plasma optical emission spectroscopy (ICP-OES) analysis was performed on a PerkinElmer Optima 8300 ICP-OES spectrometer to determine actual metal weight loadings for each catalyst. Nitrogen physisorption was carried out on a Micromeritics APAP 2020 with surface area and porosimetry analyzer to measure the surface areas and pore volume of samples. Powder X-ray diffraction (XRD) was employed to analyze material phases of catalysts. Before analysis, the samples were reduced for 1 h at the same temperature used in synthesis. XRD data were collected on a Rigaku Smart Lab automated powder diffraction system using Cu K α radiation operated at 40 kV and 40 mA. Transmission

Table 1
Physicochemical properties of samples.

Sample	Metal Loading (wt%)		Dispersion (%)	Overlayer Coverage (%)	Particle Size (nm) ^a	Acidity (peak area) ^b	S_{BET} ($\text{m}^2 \text{g}^{-1}$)	Pore Volume ($\text{cm}^3 \text{g}^{-1}$)
SiO ₂ -Al ₂ O ₃						0.79	475	0.70
Ni/SiO ₂ -Al ₂ O ₃	5.10	Ni	3.6		19	0.60	447	0.62
Ni@Pd SD	0.260	Pd	2.4	100	17	0.51	433	0.58
Ni-Pd Bimetallic	5.02	Ni	7.7		13	0.54	409	0.61
	0.280	Pd						
Ni@Pt SD	0.0958	Pt	3.1	29	16	0.53	430	0.62
Ni-Pt Bimetallic	4.93	Ni	6.8		15	0.51	422	0.57
	0.170	Pt						
Pd (Reactivity)	0.489	Pd	30		5.1	0.47	441	0.68
Pd (Isotherms)	4.98	Pd	12					
Pt (Reactivity)	0.476	Pt	16		7.5	0.48	465	0.68
Pt (Isotherms)	4.96	Pt	15					

^a Calculated from XRD using the Scherrer equation.

^b NH₃-TPD desorption.

electron microscopy (TEM) was performed on a FEI Tecnai G2 F20 S-Twin 200 kV transmission electron microscope. The temperature programmed oxidation of spent samples was evaluated by using 20% O₂/N₂ with a mass spectrometer detector. The temperature was increased from room temperature to 900 °C using a 10 °C/min ramp rate. NH₃ temperature programmed desorption (NH₃-TPD) was conducted to evaluate the acidity of catalysts. Typically, samples (200 mg) loaded in the quartz tube were treated with pure nitrogen gas at 350 °C for 1 h. After pretreatment, the samples were exposed to 5.0% NH₃ in N₂ at 100 °C for 1 h. Then, the weakly adsorbed NH₃ was removed from samples by purging pure nitrogen gas at 100 °C for 1 h. The desorption was performed by increasing the temperature to 700 °C with a ramp rate of 10 °C/min and the desorbed NH₃ was detected with a Hiden HPR20 mass spectrometer system using the signal of m/e = 16. Hydrogen chemisorption studies were performed on a Micromeritics APAP 2020C instrument using a static volumetric technique. Prior to analysis, samples were reduced at 400 °C under flowing hydrogen. The lower temperature (400 °C) was used to minimize the potential for agglomeration during the multiple isotherm measurements. Isotherms were obtained at temperatures between 35 °C and 300 °C with pressures ranging from 1 mTorr to 900 Torr. Metal dispersions were estimated assuming chemisorption stoichiometry of H/M_{surf} = 1. Ethylene hydrogenation reaction was conducted as a descriptor reaction as described previously [50].

2.3. Guaiacol hydrodeoxygenation experiments

The HDO activity of the catalysts were studied in a fixed-bed tubular quartz reactor (i.d.=8 mm and l=400 mm) operated at atmosphere pressure and a temperature ranging from 350 to 450 °C, with pure guaiacol (Aldrich, >99%) as feedstock. In a typical experiment, 200 mg of catalyst sample was mixed with ~800 mg of silica (Alfa Aesar, 106–212 μm). Before reaction, the catalysts were reduced in the reactor with a flow of pure hydrogen (60 mL/min) at 450 °C. During catalytic tests, the pure guaiacol liquid was introduced by a HPLC pump at a rate of 0.72 mL/h and the hydrogen flow rate was 60 mL/min (the molar ratio of H₂ to guaiacol was about 25). Liquid samples collected by cold trap at 1 h intervals were analyzed off-line by gas chromatograph (Thermo-Fisher Trace GC Ultra) equipped with a flame ionization detector (FID) and Rt-Q-BOND column for product analysis. The 2-isopropylphenol as internal standard was added into the collected liquid samples before analysis.

Product selectivity was calculated as $S_i(\%) = (\text{Mol}_{\text{product-}i}/\text{Mol}_{\text{reactedguaiacol}}) \times 100\%$. Turn over frequency (TOF) was calculated as described in the following. For monometallic (Ni, Pd and Pt) and non-structured (Ni-Pd and Ni-Pt) bimetallic catalysts, total active sites for TOF calculation were calculated based on surface metal atoms from dispersion. For overlay catalysts, we assumed that all measured palladium or platinum loading is on the surface. As the Pd loading was enough for 100% coverage of Ni@Pd overlay catalysts, surface metal atoms calculated from dispersion was used for TOF calculation. For Ni@Pt overlay catalysts, Pt coverage was less than 100% coverage, and the amount of Ni active sites on the surface was calculated by subtracting the Pt active sites from the total surface metal atoms. It was also assumed that Ni active sites on Ni@Pt overlay catalysts have the same activity for guaiacol conversion as that of Ni active sites on monometallic Ni catalyst. Therefore, the guaiacol conversion by Pt active sites could be calculated by subtracting the conversion by Ni active sites from the total guaiacol conversion. Then the activity of Pt active sites on overlay catalysts was calculated.

3. Results and discussion

3.1. Physicochemical properties

The metal weight loadings, dispersions, calculated percent overlay coverage, surface areas and pore volumes for catalysts are summarized in Table 1. For Ni@Pd and Ni@Pt overlay samples, Pt or Pd was successfully loaded on the overlay catalysts. As shown in Table 1, non-structured bimetallic Ni-Pd and Ni-Pt catalysts were also synthesized with metal loadings similar to that

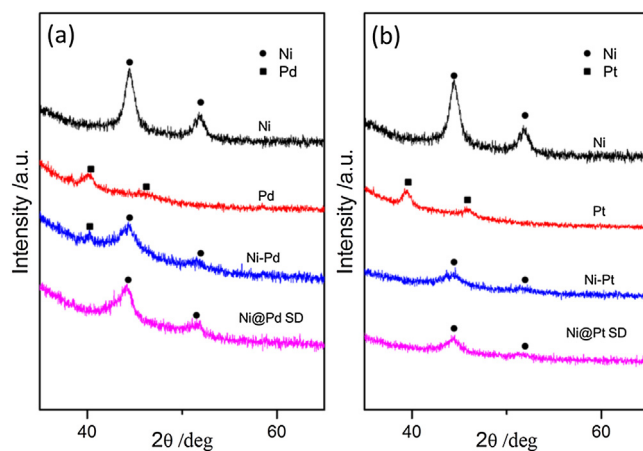


Fig. 1. XRD patterns of SiO₂-Al₂O₃ supported (a) Ni and Pd based catalysts and (b) Ni and Pt based catalysts.

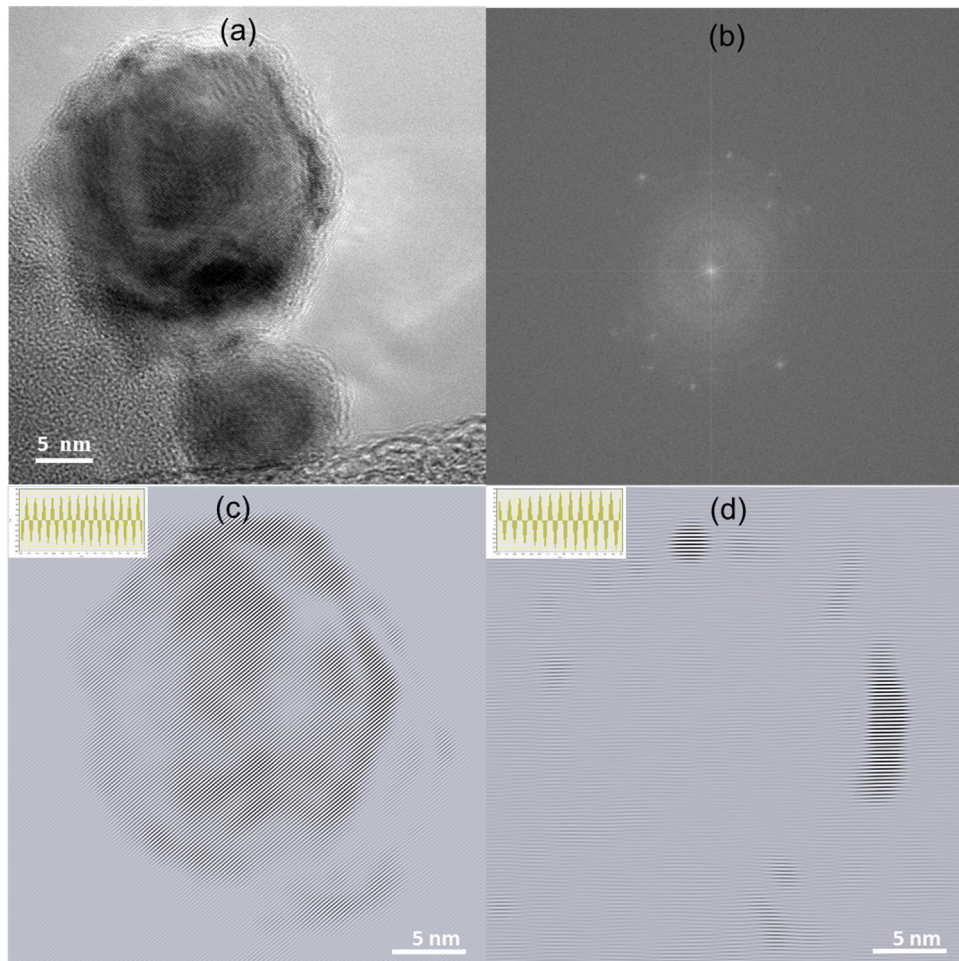


Fig. 2. (a) HRTEM image of Ni@Pd SD overlayer particle, (b) the Fourier transform of image (a), (c) Inverse Fourier transform showing inside lattice fringes, (d) Inverse Fourier transform showing lattice fringes around the particle.

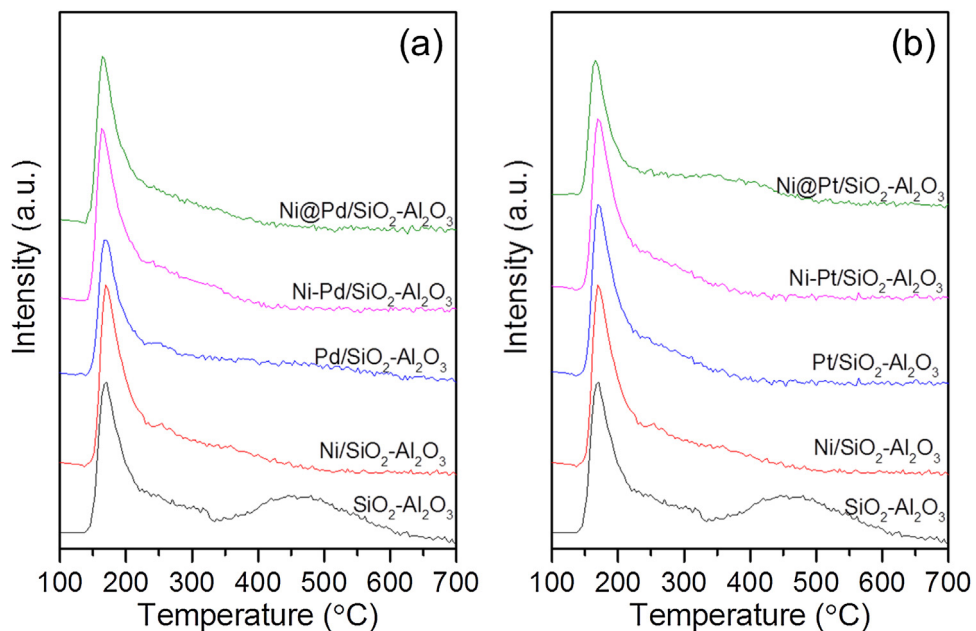


Fig. 3. NH₃-TPD profiles of SiO₂-Al₂O₃ and SiO₂-Al₂O₃ supported (a) Ni and Pd based catalysts and (b) Ni and Pt based catalysts.

of their respective Ni@Pd or Ni@Pt counterparts for direct comparison. According to Ni–Pd and Ni–Pt phase diagrams, at these concentrations the Pd and Pt should be completely miscible in the Ni without forming a second phase [56,57]. Compared with Ni parent catalyst, adding Pd or Pt increases the metal dispersion of both non-structured bimetallic Ni–Pd and Ni–Pt catalysts. Nitrogen physisorption results showed that all catalysts had similar surface area ($410\text{--}460\text{ m}^2\text{ g}^{-1}$) and pore volume ($0.57\text{--}0.68\text{ cm}^3\text{ g}^{-1}$). For overlayer samples, Pd or Pt deposition only slightly decreased the surface area and pore volume.

3.2. Powder XRD

Fig. 1 shows the results of X-ray diffraction investigation of $\text{SiO}_2\text{-Al}_2\text{O}_3$ supported catalysts. For Ni and Pd system (shown in **Fig. 1(a)**), peaks of metallic Ni were observed in all samples containing Ni. Metallic Pd peaks were observed in the Ni–Pd bimetallic sample, which suggests that isolated Pd only domains exist in the randomly-structured bimetallic Ni–Pd sample. The metallic Pd peak wasn't observed in Ni@Pd overlayer sample in spite of the Pd weight loading being equivalent or greater than the Ni–Pd sample. The Pd atoms in Ni@Pd overlayer appear to be present in non-agglomerated structures that are not detectable by XRD. This also indicates that Pd in the Ni@Pd overlayer sample is present in a different structure than the bimetallic Ni–Pd catalyst. For Ni–Pt system (shown in **Fig. 1(b)**), a metallic Pt peak was not observed in Ni–Pt. Again, no evidence of Pt only domains was observed for the Ni@Pt overlayer sample.

3.3. TEM study

Fig. 2(a) shows TEM image of a Ni@Pd SD overlayer particle deposited on silica alumina support. As shown in **Fig. 2(b)**, the Fourier transform of this image indicates that it has crystalline structure. After performing the inverse Fourier transform of different pairs of sharp spots (from **Fig. 2(b)**) in reciprocal space, two different types of lattice fringes (see **Fig. 2(c)** and (d)) were observed. One type of lattice fringes were inside the edge of the particle (**Fig. 2(c)**) and the other type showed the lattice fringes around the particle edge (**Fig. 2(d)**). The lattice spacing inside the edge of the particle (from the inset in **Fig. 2(c)**) is approximately 0.21 nm , which is consistent with the planar distance spacing of Ni(111) and the fringes inside the edge of the particle likely represent Ni. The lattice spacing around the particle edge (from the inset in **Fig. 2(d)**) is approximately 0.23 nm , which is slightly larger than bulk Pd(111) planar distance spacing (0.225 nm). Teranishi et al. observed that the interplanar spacing of Pd(111) could vary from 0.225 nm to 0.229 nm among different size palladium nanoparticles [58]. The larger lattice fringe around the particle similar to Pd spacing values indicates that the Ni@Pd overlayer was successfully prepared. Regardless, the TEM images provide evidence for a core/shell type structure. However, further characterizations are needed to provide additional evidence for overlayer catalyst structure.

3.4. Acidity of catalysts

$\text{NH}_3\text{-TPD}$ was conducted to compare the acidity of catalysts. The $\text{NH}_3\text{-TPD}$ desorption profiles are shown in **Fig. 3** and the relative peak areas are presented in **Table 1**. The $\text{NH}_3\text{-TPD}$ profiles of $\text{SiO}_2\text{-Al}_2\text{O}_3$ support showed three major peak areas at $T < 200^\circ\text{C}$, $200\text{--}400^\circ\text{C}$ and $400\text{--}600^\circ\text{C}$, which can be described as NH_3 desorption from weak, medium and strong acid sites, respectively [59]. All supported catalysts showed very similar $\text{NH}_3\text{-TPD}$ profiles with a major desorption peak at around $165\text{--}170^\circ\text{C}$. All supported catalysts showed only small amounts of desorption at $400\text{--}600^\circ\text{C}$ compared to the pure support, indicating fewer strong

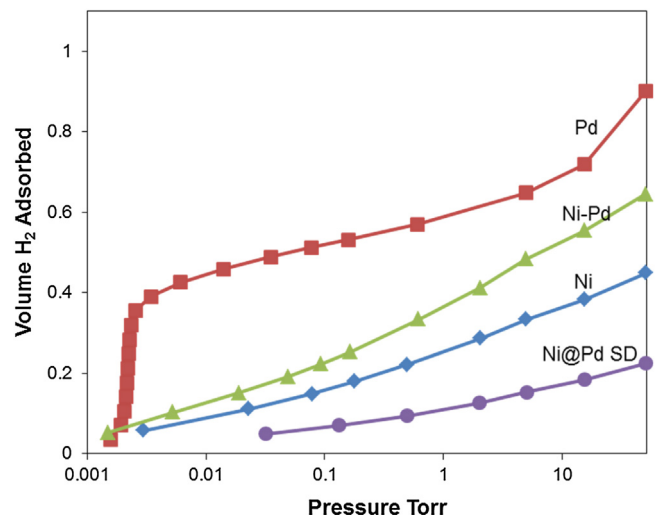


Fig. 4. Log-scale H_2 isotherms for Pd, Ni, Ni@Pd and Ni–Pd catalysts at 50°C .

acid sites compared to the support. The total amount of acidity were compared by using relative desorption peak areas (**Table 1**). All supported catalysts had similar total peaks area (0.47–0.60), which is expected since the same support was used for all catalysts and the deposited metal only covers a very small fraction of the surface. Thus, there does not appear to be any clear difference in the support acidity resulting from the overlayer synthesis. This indicates that any observed activity changes are likely due to changes in the metallic aspect of the catalysts. The total desorption peak areas were obtained by integrating the peak areas from 100 to 650°C .

3.5. Hydrogen chemisorption

Fig. 4 shows isotherms of hydrogen adsorption on Ni@Pd overlayer and bimetallic based catalysts at 50°C in comparison to palladium and nickel only catalysts. Comparing with other catalysts, the monometallic Pd showed a strong initial/low pressure (below 0.01 Torr) adsorption. In contrast with the Pd, Ni only catalyst shows little low pressure adsorption and a nearly linear (plotted on a semi-log scale) increase in adsorption across all pressures. Unlike the Pd only catalyst showing a strong initial/low pressure adsorption, Ni@Pd overlayer catalyst didn't have this strong initial adsorption and shows a lower slope than Ni parent. Nickel platinum system (in **Fig. 5**) showed similar behavior as nickel palladium based catalysts. Pt and Ni–Pt show some low pressure adsorption, and the overlayer sample didn't have this low pressure adsorption. These chemisorption results demonstrated that Pd and Pt behavior can be modified via overlayer synthesis, and Ni@Pd and Ni@Pt overlayer both showed a decrease in H_2 adsorption as computationally predicted. This agrees with our previous study on alumina supported Ni@Pt and Co@Pt catalysts [50].

The hydrogen heat of adsorption was calculated from isotherms at multiple temperatures via the Clausius–Clapeyron equation as described in the literature [49]. **Figs. 6 and 7** show hydrogen heat of adsorption values as a function of quantity of adsorbed hydrogen for silica-alumina supported catalysts. The maximum heat of H_2 adsorption for Pd catalyst was 65 kJ mol^{-1} , which compares favorably with the reported values of 61 and 67 kJ mol^{-1} [60]. The Pt catalyst had a maximum heat of H_2 adsorption value of 52 kJ mol^{-1} , which was similar to a reported 58 kJ mol^{-1} for silica alumina supported Pt catalyst with a dispersion of 74% [52,61]. As shown in **Figs. 6 and 7**, heats of H_2 adsorption were reduced by Ni@Pt and Ni@Pd overlayer synthesis when compared to parent metal (Ni) and monometallic Pd or Pt only catalysts. Decreased hydrogen adsorp-

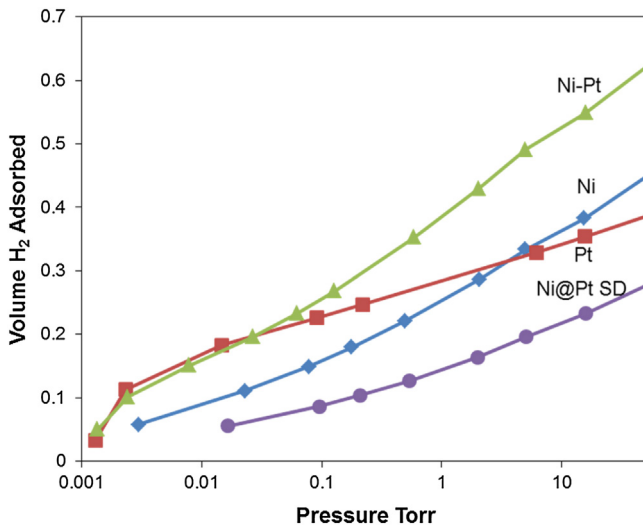


Fig. 5. Log-scale H₂ isotherms for Pt, Ni, Ni@Pt and Ni–Pt catalysts at 50 °C.

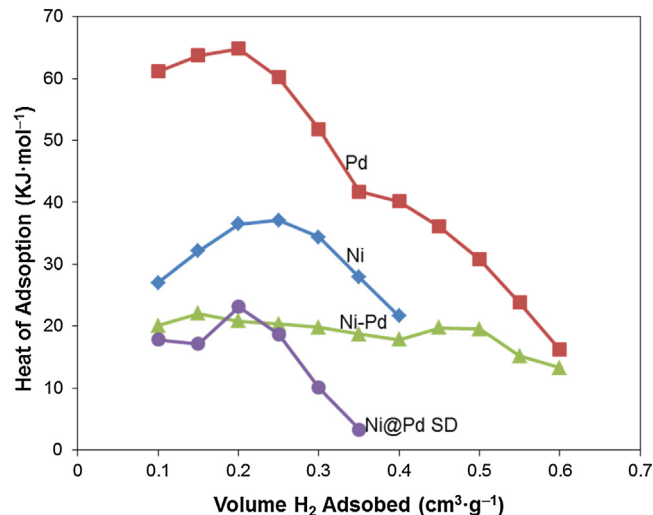


Fig. 6. Isosteric heat of H₂ adsorption for SiO₂–Al₂O₃ supported Ni and Pd based catalysts as function of volume adsorbed.

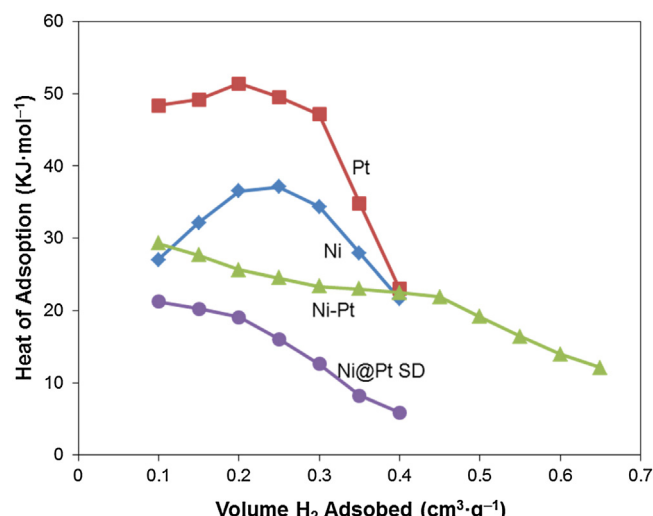


Fig. 7. Isosteric heat of H₂ adsorption for SiO₂–Al₂O₃ supported Ni and Pt catalysts as function of volume adsorbed.

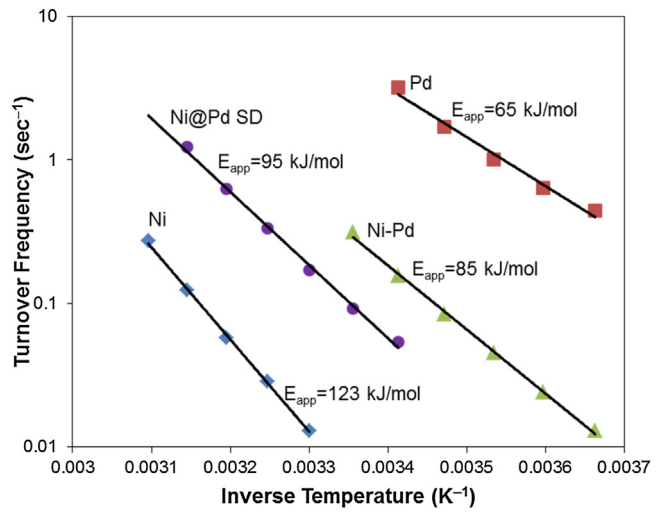


Fig. 8. Arrhenius-type plot for ethylene hydrogenation on silica-alumina supported Ni and Pd based catalysts.

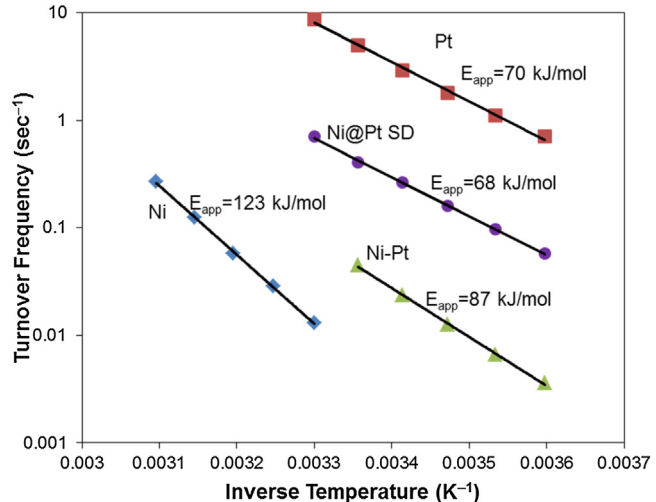


Fig. 9. Arrhenius-type plot for ethylene hydrogenation on silica-alumina supported Ni and Pt based catalysts.

tion strength of the Pd or Pt overlayer catalyst compared to the pure Pd or Pt is consistent with computational studies which predict Ni@Pd or Ni@Pt overlayer catalyst will bind hydrogen more weakly than monometallic Pd or Pt due to surface metal d-band shift [45–47]. The observed decrease in heat of adsorption also provides evidence that the desired surface structure was formed. This reduction in hydrogen and other reactant or product adsorption strength is expected to decrease bonding strength slightly, so that fewer surface sites are covered and thus enhance the HDO activity.

3.6. Ethylene hydrogenation results

Ethylene hydrogenation represents a simple descriptor reaction where the rate has been shown to be dependent on hydrogen binding strength [47,49]. Results of ethylene hydrogenation studies can be seen in the Arrhenius-type plots shown in Figs. 8 and 9. The Weisz–Prater criterion was evaluated and it indicates a lack of significant intra-phase diffusion effects during the ethylene hydrogenation reaction over all the samples. The detailed calculation process is described in the Supplementary data. Ethylene hydrogenation turnover frequencies for monometallic catalysts and non-structured bimetallic Ni–Pd catalysts were calculated

based on surface active sites (from dispersion). Overlayer catalysts' turnover frequencies were calculated using the measured palladium or platinum loading with an assumed dispersion of 100%. For core@shell catalysts, if the palladium or platinum loading, with an assumed dispersion of 100%, exceeded 100% surface coverage, the total surface active sites from dispersion were used for turnover frequency calculation. For overlayer catalysts (shown in Figs. 8 and 9), the overlayer sample showed an increased activity of at least one order of magnitude when compared to the parent Ni. This indicates that the directed deposition synthesis is adding palladium or platinum to the surface of the catalysts, thus shifting the reactivity behavior toward that of the palladium or platinum only catalyst. The significant activity difference between the parent (Ni) and overlayer (Pt or Pd) supports the above method in calculating TOF of the overlayer catalysts. Moreover, the core@shell catalysts were less active than pure palladium or platinum sample, which indicates that core@shell catalysts result in reduced hydrogenation reactivity. Reduced activity is in agreement with H₂ chemisorption results that overlayer samples exhibited a significantly lower heat of adsorption than the monometallic Pd or Pt sample. For Ni and Pd based catalysts, the non-structured Ni–Pd sample was active at the same temperature range as the Pd only catalyst, suggesting that all activity was due to Pd only domains on the support surface, which have been shown to exist via observed metallic Pd XRD peak in Ni–Pd sample. The low activity of the Ni@Pd overlayer sample at these temperature suggests that the Pd is only atop Ni particles and is likely not isolated as Pd only domains as in the non-structured Ni–Pd bimetallic catalyst. For Ni and Pt based catalysts, Ni@Pt overlayer catalyst also showed reduced hydrogenation reactivity compare to the Pt catalyst. In sum, overlayer samples demonstrated a reduced reactivity compared with palladium or platinum only catalysts, which is consistent with computational predictions and previous studies by our lab [43,49,50]. Based on the literature results that suggest strong bonding inhibit the HDO reaction, we have identified Ni@Pd and Ni@Pt catalysts with reduced adsorption strength as potential candidates for guaiacol HDO and these catalysts were further tested for in guaiacol HDO.

Apparent activation energy for each catalyst was calculated based on the Arrhenius-type plots and are provided in Figs. 8 and 9. The apparent activation energies for the Pd and Pt monometallic catalysts were 65 and 70 kJ mol⁻¹, respectively. These numbers were within the range of various values reported in literature [50,52,60,62–64]. Ni@Pd SD overlayer catalyst showed an apparent activation energy of 95 kJ mol⁻¹, which is much higher than Pd catalyst. Unlike Ni@Pd SD overlayer catalyst, Ni@Pt SD overlayer catalyst had a value of 68 kJ mol⁻¹, slightly lower than Pt catalyst. Both overlayer catalysts showed different apparent activation energies with their non-structured bimetallic counterparts, further confirming that overlayer catalyst show different properties compared to non-structured bimetallic catalysts.

Fig. 10 shows the correlation between the heat of H₂ adsorption at the hydrogen coverage of 0.1 cm³ g⁻¹ and the TOF of ethylene hydrogenation at 293 K for studied palladium, platinum and overlayer catalysts. The ethylene hydrogenation reaction has been reported to have positive reaction order with respect to H₂, which suggests that reactivity and H₂ surface coverage are positively correlated [52,63]. Therefore, decreased hydrogen adsorption strength is anticipated to reduce the hydrogen coverage on the catalyst surface and thus decrease the ethylene hydrogenation reaction rate. The correlation in Fig. 10 demonstrates a positive correlation between ethylene hydrogenation reactivity and the H₂ adsorption strength, and also demonstrates that ethylene hydrogenation can be used as a descriptor reaction for H₂ binding strength for overlayer catalysts.

3.7. Hydrodeoxygenation of guaiacol

For the HDO of guaiacol, both the support and metal are required for high activity. In this work, we are examining the ability of overlayer catalysts to improve the reactivity of the metal. In an effort to isolate the study to the metal, an identical support was used for all catalysts. BET surface area and pore volume measurements showed only minor changes in the support for the different catalysts. Thus, it is likely that the support is acting similarly for all catalysts

The supported catalysts were evaluated for the HDO of guaiacol at 350 °C, 400 °C and 450 °C at atmospheric pressure. Blank-reactor runs showed a negligible activity for guaiacol at reaction condition, less than 0.5% conversion (not shown). As the pure Pd and Pt catalysts showed much higher dispersion than other catalysts, 0.5 wt% metal loading Pd and Pt only catalysts were used for HDO test to keep the number of active sites similar. The conversion and selectivity results of guaiacol hydrodeoxygenation on different catalysts are presented in Table S1. The Weisz–Prater criterion was evaluated and it indicates a lack of significant intra-phase diffusion effects during the guaiacol HDO reaction over all the catalysts. The detailed calculation process is described in the Supplementary data. Selectivity of the deoxygenation products were given separately, while selectivity of all non-deoxygenation products (molecules with two oxygen atoms) was reported as “others”. The support showed small guaiacol conversion with non-deoxygenation products (“others”) as major products (see Table S1). For all tested catalysts, the main deoxygenation product was phenol (loss of a methoxy group) under reaction condition. Some studies have reported phenol to be either a main product or an intermediate for further deoxygenation in guaiacol deoxygenation [21,26,39,41]. Other major deoxygenation products included cresol (conversion of the methoxy to a methyl group), while small amounts of anisole (loss of a hydroxyl group) were observed. The formation of cresol (loss of a hydroxyl) is related to the reaction of methyl substitution in HDO of guaiacol, which was due to the acidity of the support, because the acidity of support has been found to have a key effect on the reaction of methyl substitution in HDO of guaiacol [29,65,66]. Detectable benzene was also found at some reaction

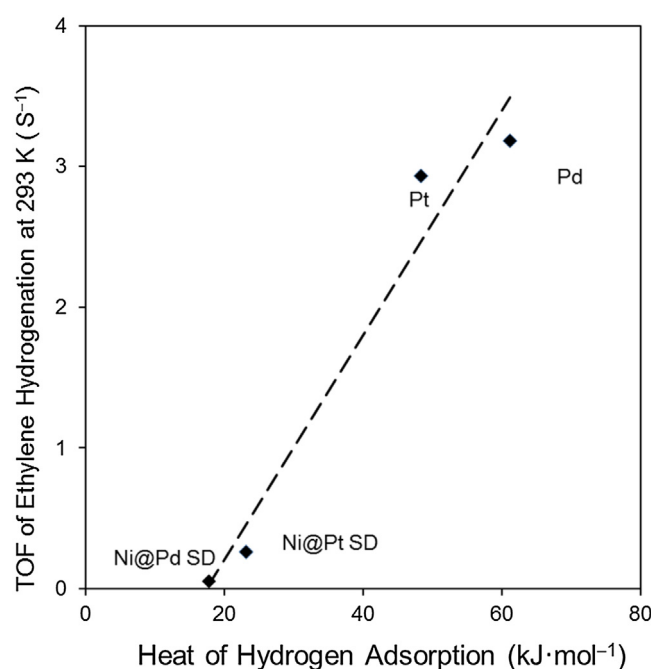


Fig. 10. Correlation between H₂ heat of adsorption and TOF of ethylene hydrogenation on studied overlayer catalysts, pure palladium and platinum catalysts.

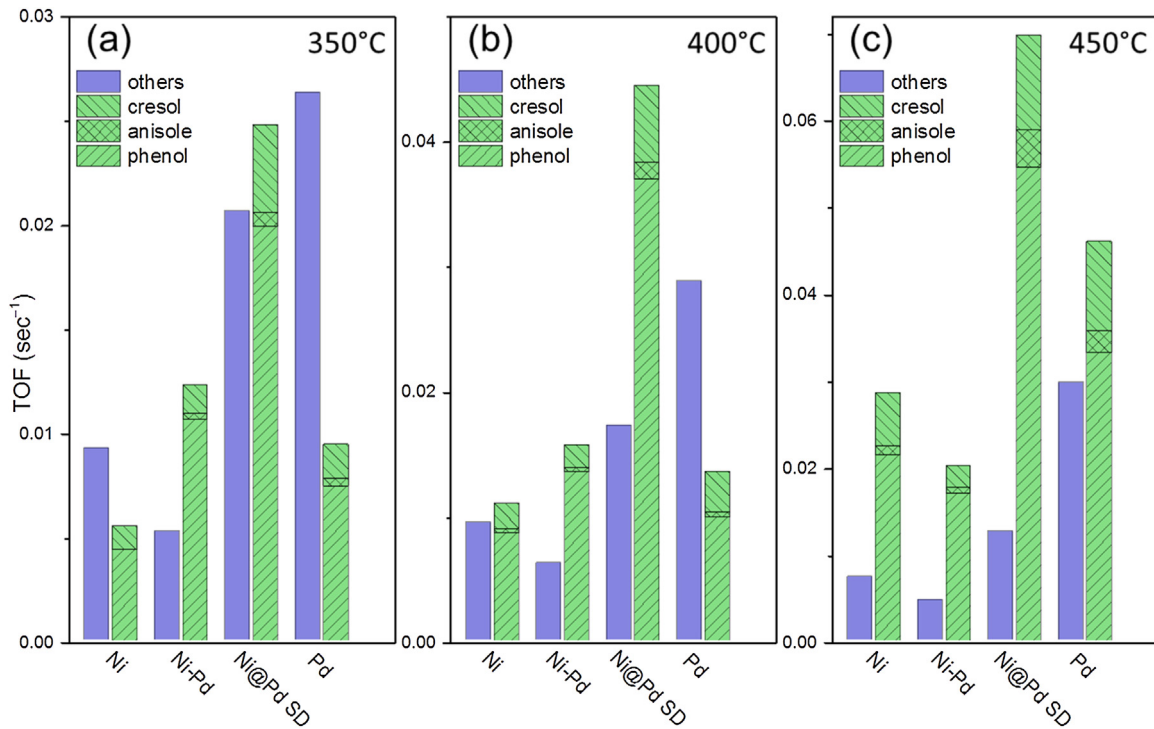


Fig. 11. TOFs of guaiacol deoxygenation and non-deoxygenation product formation over Ni and Pd based catalysts at (a) 350 °C, (b) 400 °C, (c) 450 °C.

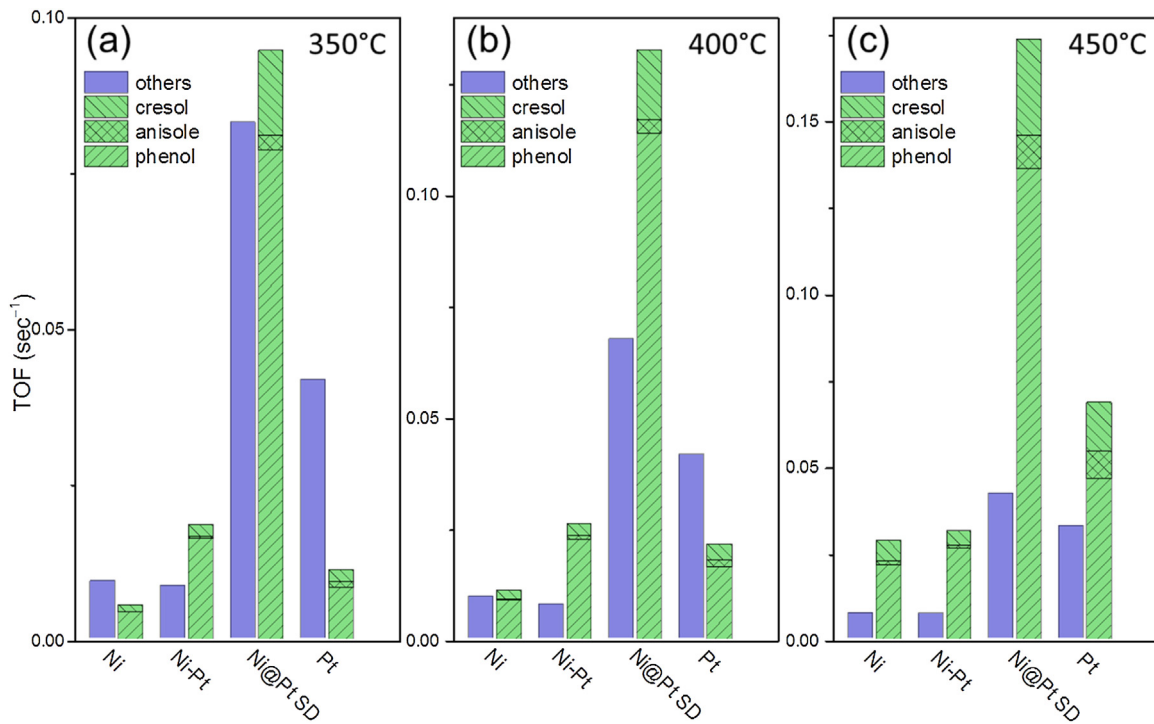


Fig. 12. TOFs of guaiacol deoxygenation and non-deoxygenation product formation over Ni and Pt based catalysts at (a) 350 °C, (b) 400 °C, (c) 450 °C.

conditions. No ring saturated products (cyclohexane derivatives) were observed under tested reaction conditions. Compared with Ni parent and monometallic Pd and Pt catalysts, the bimetallic catalysts and overlayer catalysts showed higher guaiacol conversion and deoxygenation product selectivity. For monometallic Pd and Pt catalysts, more than 65% of products at 350 °C and 400 °C were non-deoxygenation products ("others" in Table S1). Both bimetallic catalysts and overlayer catalysts improved catalyst selectivity

greatly, enhancing the selectivity toward the production of the desired deoxygenation products. However, at the highest temperature of 450 °C, these improvements were not as remarkable as at low temperature.

In order to illustrate more clearly the difference in production rates of active sites on catalysts, the turnover frequency (TOF) of deoxygenation and non-deoxygenation products were calculated and presented in Fig. 11 and 12. As shown in Fig. 11, the column

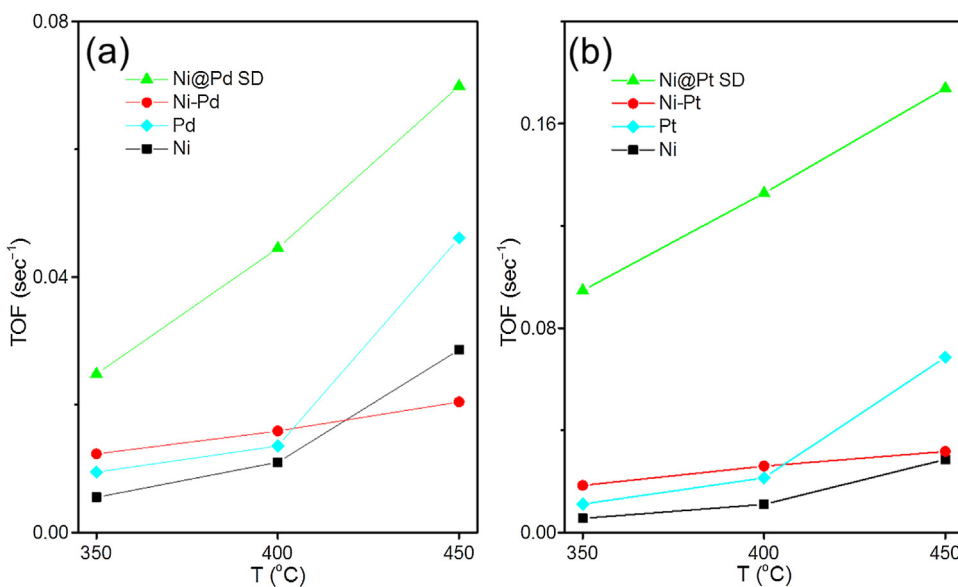


Fig. 13. TOFs of guaiacol deoxygenation products over (a) Ni and Pd based catalysts, (b) Ni and Pt based catalysts at different reaction temperature.

in green color (second column) shows the TOF of deoxygenation products, which is the sum of all detected deoxygenation products including anisole, o-cresol and phenol. Though the monometallic Pd catalyst had the highest TOF of non-deoxygenation product formation at 350 °C, its TOF of deoxygenation product formation was the second lowest. The Ni–Pd catalyst has the highest guaiacol conversion and deoxygenation product yield among Ni, Pd, Ni–Pd and Ni@Pd overlayer catalysts at 350 °C, however its TOF of deoxygenation products was only half that of the overlayer catalyst, indicating that the high guaiacol conversion on Ni–Pd catalyst was mainly due to the high metal dispersion. Among the tested catalysts at 350 °C (Fig. 11(a)), the TOF of deoxygenation product formation of Pd active sites on Ni@Pd overlayer catalyst was the highest, about 3 times as high as that of the monometallic Pd catalyst (whose behavior the overlayer is designed to modify) and 5 time as high as that of the Ni catalyst. The result, that Pd active sites on Ni@Pd overlayer catalysts had higher TOF of deoxygenation product formation than monometallic Ni and Pd catalysts, is consistent with the postulate that Pd active sites on Ni@Pd overlayer catalyst might have higher HDO activity than the monometallic Pd due to the decrease in hydrogen and hydrocarbon adsorbate binding strengths. As shown in Fig. 12, the Ni@Pt, Ni–Pt and Pt catalysts showed a similar HDO activity trend compared to the Ni@Pd, Ni–Pd and Pd catalysts. The Pt active sites on Ni@Pt overlayer catalyst showed higher TOF of deoxygenation product formation than monometallic Ni and Pt catalysts. From the aforementioned results, it is clear that the Pd or Pt active sites of Ni@Pd and Ni@Pt overlayer catalysts show much higher deoxygenation activity than that of Ni, Pd, Pt, Ni–Pd and Ni–Pt samples. These result support the postulate that Ni@Pd and Ni@Pt overlayers with decreased binding strength would improve performance for the HDO reaction.

As shown in Figs. 11 and 12, reaction temperature had a strong effect on HDO of guaiacol. For all catalysts, the guaiacol conversion and deoxygenation product selectivity increased as the temperature was increased to 400 °C and 450 °C, while selectivity of non-deoxygenation decreased with increasing temperature. This result is in good agreement with other literature reports [67,68]. Under our reaction condition, no ring-saturation products were observed even at 450 °C. This is desirable, for aromatic products are more attractive than ring-saturation products for further application and to reduce H₂ consumption [3,21,69]. Several previous studies with similar reaction conditions also did not observe ring-

saturation products as well [39,70]. Sun et al. reported that, for carbon supported precious metals catalysts, ring-saturation products observed at 250 °C were not observed after temperature had been increased above 350 °C due to ring opening to form C1 products at high reaction temperature [41]. However, this situation does apply to our case, where no C1 products were observed beside small amount of methanol (<1%). Recently, Tran et al. proposed that high reaction temperature (400 °C) and low reaction pressure could prevent the hydrogenation/dehydrogenation for ring saturation [70]. Again for all catalysts, the TOFs of deoxygenation products increased with temperature increasing from 350 °C to 450 °C, as shown in Fig. 13. In contrast, except for the single deposition overlayer catalyst, the TOFs of non-deoxygenation products decreased slightly from 350 °C to 450 °C. Above results suggest that further deoxygenation of phenolic products is more facile at higher temperature than at low temperature for silica aluminum supported catalysts. Overlayer catalysts showed the highest TOFs of deoxygenation among tested catalysts with temperature from 350 °C to 450 °C.

Catalyst stability is also important for HDO applications. Some studies have reported that the bimetallic catalyst could improve catalyst stability [39,71]. A Au–Pt bimetallic surface with weaker binding energies of adsorbates than Pt was also reported to inhibit carbon deposition on the surface [72]. To gain insights into how overlayer catalysts affect the stability of the catalysts, all catalysts were tested for guaiacol HDO reaction at 450 °C for 6 h. The variations of guaiacol conversion and product selectivity at 450 °C as a function of time on stream (TOS) are compared in Fig. 14 and Fig. S1. As shown in Fig. 14, for Pd only catalyst, the selectivity of non-deoxygenation product decreased with TOS from 1 h to 4 h, and the selectivity of phenol and o-cresol increased slightly with TOS. For Ni and Ni@Pd overlayer catalyst, selectivity of non-deoxygenation remained stable with TOS, while selectivity of phenol decreased slightly within first 3 h and then kept stable. The selectivity of o-cresol on Ni and Ni@Pd overlayer catalyst increased slightly with TOS as that of the Pd only catalyst. The axis on the right side of Fig. 14 is for conversion. The scale of conversion for Ni–Pd and Ni@Pd overlayer is different from that for Ni and Pd. Unlike selectivity, the conversion of guaiacol on Ni and Pd based catalyst decreased with TOS. For all Ni and Pd based catalysts, the guaiacol conversion dropped to around forty percent of initial guaiacol conversion after a reaction time of 6 h. Severe deactivations for guaiacol HDO caused

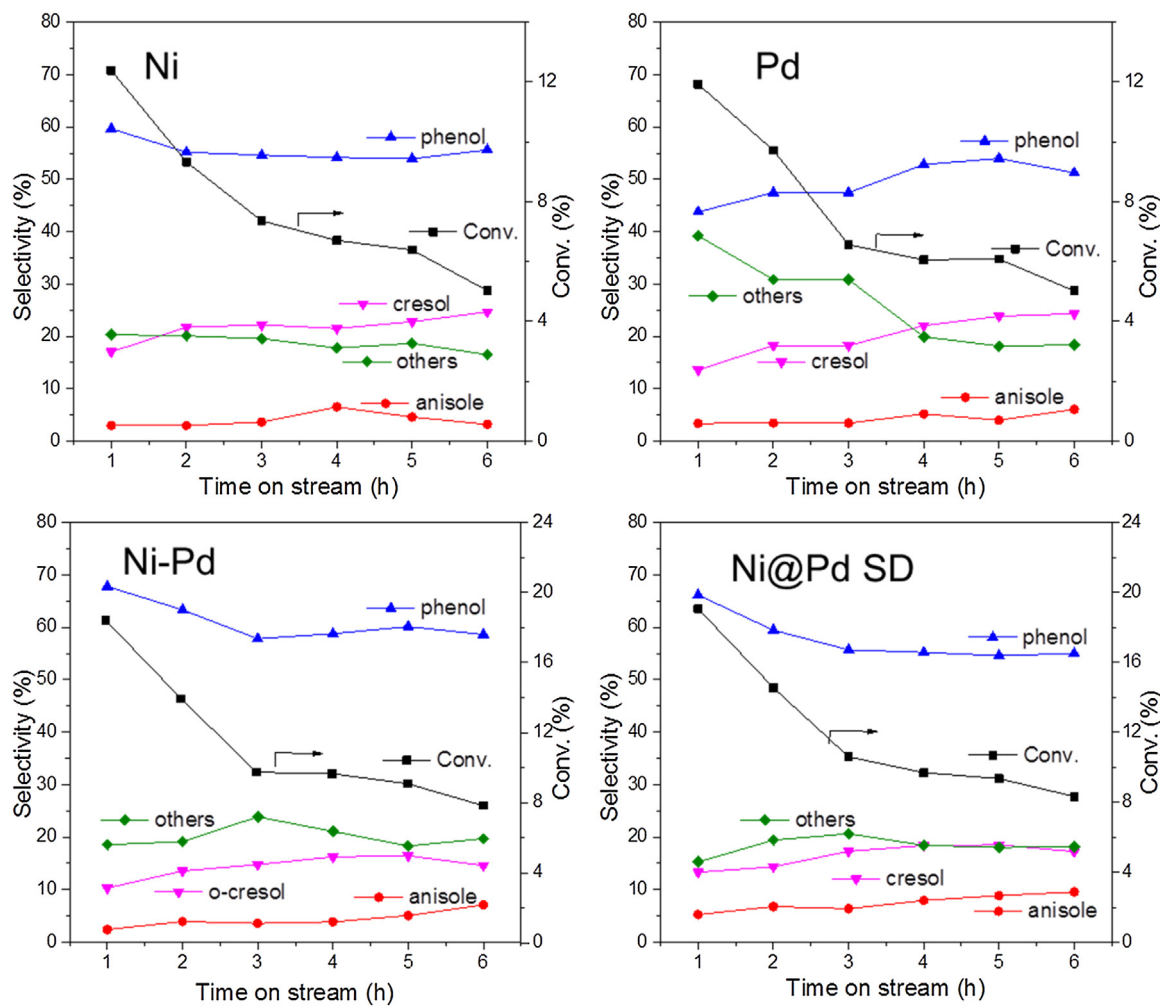


Fig. 14. Conversion of guaiacol and product selectivity over Ni and Pd based catalysts as function of time on stream.

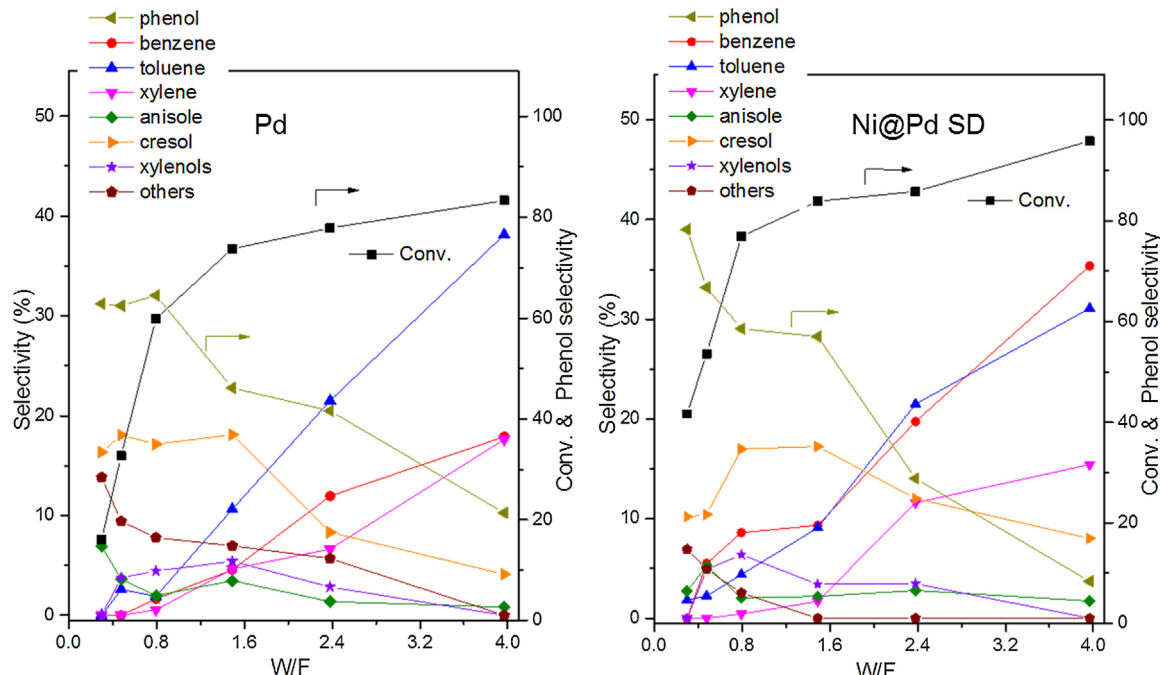


Fig. 15. Conversion of guaiacol and product distribution over Pd and Ni@Pd SD catalysts as a function of W/F at 30 min.

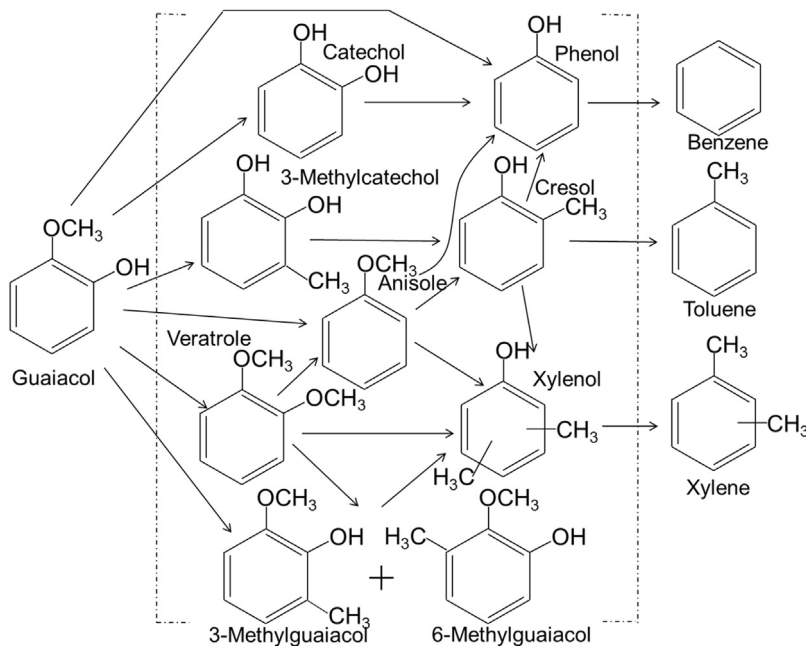


Fig. 16. Guaiacol HDO reaction pathways over silica-alumina supported metal catalyst.

by coking were observed for different kinds of catalyst [20,21,39]. As shown in Fig. S1, the Ni and Pt based catalysts showed similar stabilities as Ni and Pd based catalysts. Metal loading, acidity and pore structure of support were proposed to affect coke deposition [29]. Since our catalyst showed similar surface area and pore volume and similar deactivation ratio with same time, we propose that the catalysts deactivation for these catalysts is mainly due to coking caused by the acidity of the support [29,73]. Silica-alumina supported Ni@Pd overlayer catalyst with a similar support acidity property to silica-alumina supported Ni, Pd and Ni–Pd catalysts couldn't enhance catalyst stability. The temperature programmed oxidation was used to investigate the coke deposition of spent catalysts after 6 h of reaction at 450 °C and the results are presented in Fig. S2. A broad CO₂ peak from around 250 °C to 700 °C was observed over Ni, Pd and Ni–Pd catalysts. The peak areas of CO₂ are very similar, suggesting similar coke deposition amount over these three catalysts. This is expected as the support was same for all three catalysts. The morphology of spent Ni@Pd SD catalyst was investigated using TEM. As shown in Fig. S3, the morphology of the catalyst didn't show any significant change with the mean particle size slightly changed from 12.1 nm to 12.4 nm after 6 h of reaction at 450 °C. This result further supports that the deactivation was due to the coke deposition.

The conversions of guaiacol over all tested catalysts were below 26% and the major deoxygenation products were incomplete deoxygenation products (phenol, anisole and o-cresol) under employed reaction conditions. This was due to the very low W/F (g of catalyst/(g of reactant h⁻¹)) employed for obtaining the TOF of the active sites, which is generally used for comparison of catalytic activity under similar reaction condition at low conversion. To achieve high guaiacol conversion and see how overlayer catalysts affect the final deoxygenation product distribution of the guaiacol HDO reaction, a range of W/F from 0.30 h to 4.0 h were tested via changing the flow rate of the feedstock which was 5 vol.% guaiacol in heptane. The overall guaiacol conversion and products distribution at different contact times and space times (W/F) on Pd only and Ni@Pd overlayer catalyst are shown in Fig. 15. It can be seen that, at very low W/F, both catalysts showed low guaiacol conversion and the major products were phenol, cresol, non-deoxygenation

products and anisole. As W/F is increased, xylenols and complete deoxygenation products like benzene, toluene, and xylene were observed. The formation of benzene, toluene, and xylene increase monotonically with W/F and in contrast, the selectivity of phenol, o-cresol, anisole, xylenols and non-deoxygenation products either decreased monotonically or went through a maximum at intermediate W/F. This implies that the phenol, o-cresol, anisole, xylenols and non-deoxygenation products are intermediate products. In contrast with the low conversion rate studies, the selectivity of the complete deoxygenated BTX (benzene, toluene, and xylene) products could be up to 82% on Ni@Pd overlayer catalyst at high W/F condition, while the Pd catalyst showed a selectivity of 73% for BTX under the same reaction condition. This agrees with results reported by Zhu et al. that benzene, toluene, and xylene were major complete deoxygenation products on Pt/HBeta catalyst [29].

Some studies have demonstrated that bimetallic catalysts can change the distribution of HDO products [38,41,71]. Our Ni@Pd overlayer catalyst with slightly reduced binding strength for reactants and intermediates also showed different deoxygenation products distribution compared with the pure Pd catalyst. Unlike the Pd only catalyst forming much more toluene than benzene, the Ni@Pd overlayer catalyst showed similar selectivity for toluene and benzene. One of the major reaction pathways for producing benzene from guaiacol is that the catechol intermediate is formed first, then phenol is produced from catechol, and finally phenol is converted into benzene [13,39,41,74,75]. The catechol with two C–OH groups usually can be strongly bonded to a catalyst surface [39]. It is proposed that the Ni@Pd overlayer catalyst with weaker adsorption strength than Pd can enhance the formation of phenol from catechol and then increase final benzene selectivity.

According to product distribution at different temperatures and product distribution with varying W/F, major reaction pathways on SiO₂–Al₂O₃ supported metals catalysts studied in this work were proposed and presented in Fig. 16. Most pathways of these proposed reaction pathways are consistent with reaction pathways previously proposed by others [13,41,74,75]. However, only a few of the literature proposed pathways included the formation of veratrole and methylguaiacol. In these proposed reaction pathways, formations of catechol, 3-methylcatechol, veratrole and methyl-

guaiacol from guaiacol were major steps at low conversion or W/F. Since xylenols and xylenes were observed as major intermediate and final complete deoxygenation products, pathways involving formation of xylenols and xylenes were also proposed in this work. A few previous proposed pathways for guaiacol HDO showed steps for formation of xylenols and xylenes. The reaction network proposed by Runnebaum et al. gave steps for formation of xylenols and xylenes, but didn't include proposed steps of formation of xylenes from xylenols [74]. Only pathways proposed by Resasco et al. for anisole HDO on Pt/HBeta included these steps [29]. Their experience showed that xylenes were only observed during HDO on Pt/HBeta, not on Pt/SiO₂. It was speculated that the acidic support can catalyze the transalkylation of oxygenated aromatics, and result in transferring methyl groups from one aromatic molecule to another aromatic molecule instead of forming methane [29,76]. Combination of the proposed reaction pathways with the production distribution results from this work under low guaiacol conversion condition tends to suggest that the catechol, 3-methylcatechol, veratrole and methylguaiacol could be major initial intermediate products. All of these three compounds having two functionalized groups with oxygen can have a strong bonding with the catalyst. We proposed that overlayer catalysts with weaker bonding strength probably enhance final HDO activity via facilitating the conversion of these intermediate products.

4. Conclusions

In this work, hydrodeoxygenation of guaiacol was studied using silica alumina supported Ni@Pd and Ni@Pt overlayer catalysts under atmospheric pressure. Hydrogen chemisorption, ethylene hydrogenation, XRD and TEM studies have demonstrated that palladium or platinum could be deposited atop supported nickel catalysts and the prepared overlayer showed behavior consistent to that of computational predictions. When normalized per active site, Pd and Pt active sites of overlayer catalysts showed significantly enhanced deoxygenation activity compared with that of Pd or Pt only catalyst. However, overlayer catalysts didn't show better stability than Ni, Pd or Pt only catalysts. Results of guaiacol HDO with different W/F showed that selectivity of benzene, toluene, and xylenes could be up to 80% on Ni@Pd overlayer catalyst at high W/F condition. In addition, major reaction pathways of guaiacol HDO on silica alumina supported metals catalysts were proposed.

Acknowledgements

The authors would like to acknowledge funding provided by the National Science foundation, Chemical, Bioengineering, Environmental, and Transport Systems [CBET-0933017]. Q. Lai and C. Zhang acknowledge support from the University of Wyoming through Energy GA awards.

Appendix A. Supplementary data

Supplementary data associated with this article can be found, in the online version, at <http://dx.doi.org/10.1016/j.apcata.2016.09.009>.

References

- [1] C.-H. Zhou, X. Xia, C.-X. Lin, D.-S. Tong, J. Beltramini, Chem. Soc. Rev. 40 (2011) 5588.
- [2] S. Czernik, A.V. Bridgwater, Energy Fuels 18 (2004) 590.
- [3] H. Wang, J. Male, Y. Wang, ACS Catal. 3 (2013) 1047.
- [4] D.M. Alonso, S.G. Wettstein, J.A. Dumesic, Chem. Soc. Rev. 41 (2012) 8075.
- [5] G.W. Huber, J.A. Dumesic, Catal. Today 111 (2006) 119.
- [6] J.D. Adjaye, N.N. Bakhshi, Fuel Process. Technol. 45 (1995) 161.
- [7] S. Vitolo, M. Seggiani, P. Frediani, G. Ambrosini, L. Politi, Fuel 78 (1999) 1147.
- [8] T.P. Vispute, G.W. Huber, Green Chem. 11 (2009) 1433.
- [9] J.C. Serrano-Ruiz, J.A. Dumesic, Energy Environ. Sci. 4 (2011) 83.
- [10] D.C. Elliott, Energy Fuels 21 (2007) 1792.
- [11] Q. Bu, H. Lei, A.H. Zacher, L. Wang, S. Ren, J. Liang, Y. Wei, Y. Liu, J. Tang, Q. Zhang, R. Ruan, Bioreour. Technol. 124 (2012) 470.
- [12] O.I. Şenol, T.R. Viljava, A.O.I. Krause, Catal. Today 106 (2005) 186.
- [13] M.V. Bykova, D.Y. Ermakov, V.V. Kaichev, O.A. Bulavchenko, A.A. Saraev, M.Y. Lebedeva, V.A. Yakovlev, Appl. Catal. B: Environ. 113 (2012) 296.
- [14] E.-J. Shin, M.A. Keane, Ind. Eng. Chem. Res. 39 (2000) 883.
- [15] Y.X. Yang, C. Ochoa-Hernandez, V.A.D. O'Shea, P. Pizarro, J.M. Coronado, D.P. Serrano, Appl. Catal. B: Environ. 145 (2014) 91.
- [16] C. Zhao, J.A. Lercher, Angew. Chem. Int. Ed. 51 (2012) 5935.
- [17] C. Zhao, S. Kasakov, J. He, J.A. Lercher, J. Catal. 296 (2012) 12.
- [18] X. Zhang, Q. Zhang, T. Wang, L. Ma, Y. Yu, L. Chen, Bioreour. Technol. 134 (2013) 73.
- [19] X. Zhang, T. Wang, L. Ma, Q. Zhang, X. Huang, Y. Yu, Appl. Energy 112 (2013) 533.
- [20] R.N. Olcese, M. Bettahar, D. Petitjean, B. Malaman, F. Giovanella, A. Dufour, Appl. Catal. B: Environ. 115 (2012) 63.
- [21] R. Olcese, M.M. Bettahar, B. Malaman, J. Ghanbaja, L. Tibavizco, D. Petitjean, A. Dufour, Appl. Catal. B: Environ. 129 (2013) 528.
- [22] M.K. Huuska, Polyhedron 5 (1986) 233.
- [23] Y. Romero, F. Richard, S. Brunet, Appl. Catal. B: Environ. 98 (2010) 213.
- [24] J. Chang, T. Danuthai, S. Dewiyanti, C. Wang, A. Borgna, ChemCatChem 5 (2013) 3041.
- [25] T. Prasomsri, M. Shetty, K. Murugappan, Y. Roman-Leshkov, Energy Environ. Sci. 7 (2014) 2660.
- [26] H.Y. Zhao, D. Li, P. Bui, S.T. Oyama, Appl. Catal. A: Gen. 391 (2011) 305.
- [27] K. Li, R. Wang, J. Chen, Energy Fuels 25 (2011) 854.
- [28] S.-K. Wu, P.-C. Lai, Y.-C. Lin, H.-P. Wan, H.-T. Lee, Y.-H. Chang, ACS Sustain. Chem. Eng. 1 (2013) 349.
- [29] X. Zhu, L.L. Lobban, R.G. Mallinson, D.E. Resasco, J. Catal. 281 (2011) 21.
- [30] A. Gutierrez, R.K. Kaila, M.L. Honkela, R. Slioor, A.O.I. Krause, Catal. Today 147 (2009) 239.
- [31] D.Y. Hong, S.J. Miller, P.K. Agrawal, C.W. Jones, Chem. Commun. 46 (2010) 1038.
- [32] J. Wildschut, F.H. Mahfud, R.H. Venderbosch, H.J. Heeres, Ind. Eng. Chem. Res. 48 (2009) 10324.
- [33] J. Wildschut, I. Melián-Cabrera, H.J. Heeres, Appl. Catal. B: Environ. 99 (2010) 298.
- [34] C. Li, X. Zhao, A. Wang, G.W. Huber, T. Zhang, Chem. Rev. 115 (2015) 11559.
- [35] W. Yu, M.D. Porosoff, J.G. Chen, Chem. Rev. 112 (2012) 5780.
- [36] J. Gao, H. Zhao, X. Yang, B.E. Koel, S.G. Podkolzin, Angew. Chem. Int. Ed. 53 (2014) 3641.
- [37] J. Gao, H. Zhao, X. Yang, B.E. Koel, S.G. Podkolzin, ACS Catal. 3 (2013) 1149.
- [38] P.T.M. Do, A.J. Foster, J. Chen, R.F. Lobo, Green Chem. 14 (2012) 1388.
- [39] M.A. Gonzalez-Borja, D.E. Resasco, Energy Fuels 25 (2011) 4155.
- [40] A.R. Ardianti, S.A. Khromova, R.H. Venderbosch, V.A. Yakovlev, H.J. Heeres, Appl. Catal. B: Environ. 117–118 (2012) 105.
- [41] J.M. Sun, A.M. Karim, H. Zhang, L. Kovarik, X.H.S. Li, A.J. Hensley, J.S. McEwen, Y. Wang, J. Catal. 306 (2013) 47.
- [42] N.A. Khan, H.H. Hwu, J.G. Chen, J. Catal. 205 (2002) 259.
- [43] E. Christoffersen, P. Liu, A. Ruban, H.L. Skriver, J.K. Nørskov, J. Catal. 199 (2001) 123.
- [44] J. Greeley, M. Mavrikakis, Nat. Mater. 3 (2004) 810.
- [45] A. Ruban, B. Hammer, P. Stoltze, H.L. Skriver, J.K. Nørskov, J. Mol. Catal. A: Chem. 115 (1997) 421.
- [46] V. Pallassana, M. Neurock, L.B. Hansen, B. Hammer, J.K. Nørskov, Phys. Rev. B 60 (1999) 6146.
- [47] V. Pallassana, M. Neurock, J. Catal. 191 (2000) 301.
- [48] M.P. Latusek, R.M. Heimerl, B.P. Spigarelli, J.H. Holles, Appl. Catal. A: Gen. 358 (2009) 79.
- [49] M.P. Latusek, B.P. Spigarelli, R.M. Heimerl, J.H. Holles, J. Catal. 263 (2009) 306.
- [50] M.D. Skoglund, C.L. Jackson, K.J. McKim, H.J. Olson, S. Sabiryanov, J.H. Holles, Appl. Catal. A 467 (2013) 355.
- [51] C. Zhang, Q. Lai, J.H. Holles, Appl. Catal. A 526 (2016) 113.
- [52] C. Zhang, Q. Lai, J.H. Holles, Catal. Sci. Technol. (2016) 11.
- [53] V.L. Barrio, P.L. Arias, J.F. Cambra, M.B. Güemez, J.M. Campos-Martin, B. Pawelec, J.L.G. Fierro, Appl. Catal. A: Gen. 248 (2003) 211.
- [54] V.L. Barrio, P.L. Arias, J.F. Cambra, M.B. Güemez, B. Pawelec, J.L.G. Fierro, Appl. Catal. A: Gen. 242 (2003) 17.
- [55] J.W. Shabaker, G.W. Huber, J.A. Dumesic, J. Catal. 222 (2004) 180.
- [56] A. Nash, P. Nash, Bull. Alloy Phase Diagr. 5 (1984) 446.
- [57] P. Nash, M.F. Singleton, Bull. Alloy Phase Diagr. 10 (1989) 258.
- [58] T. Teranishi, M. Miyake, Chem. Mater. 10 (1998) 594.
- [59] A. Aqsha, L. Katta, N. Mahinpey, Catal. Lett. 145 (2015) 1351.
- [60] M.D. Skoglund, J.H. Holles, Catal. Lett. 143 (2013) 966.
- [61] S.-C. Chou, S.-H. Lin, C.-T. Yeh, J. Soc. Chem. Faraday Trans. 91 (1995) 949.
- [62] H. Zea, K. Lester, A.K. Datye, E. Rightor, R. Gulotty, W. Waterman, M. Smith, Appl. Catal. A: Gen. 282 (2005) 237.
- [63] F. Zaera, G.A. Somorjai, J. Am. Chem. Soc. 106 (1984) 2288.
- [64] R.D. Cortright, S.A. Goddard, J.E. Rekoske, J.A. Dumesic, J. Catal. 127 (1991) 342.
- [65] T. Ninimwanwippong, R.C. Runnebaum, D.E. Block, B.C. Gates, Catal. Lett. 141 (2011) 779.
- [66] T. Ninimwanwippong, R.C. Runnebaum, D.E. Block, B.C. Gates, Energy Fuels 25 (2011) 3417.

- [67] H.Y. Zhao, D. Li, P. Bui, S.T. Oyama, *Appl. Catal. A: Gen.* 391 (2011) 305.
- [68] Y.-K. Hong, D.-W. Lee, H.-J. Eom, K.-Y. Lee, *Appl. Catal. B: Environ.* 150–151 (2014) 438.
- [69] Y. Hong, H. Zhang, J. Sun, K.M. Ayman, A.J.R. Hensley, M. Gu, M.H. Engelhard, J.-S. McEwen, Y. Wang, *ACS Catal.* 4 (2014) 3335.
- [70] N.T.T. Tran, Y. Uemura, S. Chowdhury, A. Ramli, *Appl. Catal. A: Gen.* 512 (2016) 93.
- [71] H. Ohta, B. Feng, H. Kobayashi, K. Hara, A. Fukuoka, *Catal. Today* 234 (2014) 139.
- [72] H. Ren, M.P. Humbert, C.A. Menning, J.G. Chen, Y. Shu, U.G. Singh, W.-C. Cheng, *Appl. Catal. A: Gen.* 375 (2010) 303.
- [73] P.M. Mortensen, J.D. Grunwaldt, P.A. Jensen, K.G. Knudsen, A.D. Jensen, *Appl. Catal. A: Gen.* 407 (2011) 1.
- [74] R.C. Runnebaum, T. Nimmanwudipong, D.E. Block, B.C. Gates, *Catal. Sci. Technol.* 2 (2012) 113.
- [75] V.N. Bui, G. Toussaint, D. Laurenti, C. Mirodatos, C. Geantet, *Catal. Today* 143 (2009) 172.
- [76] A. Ausavasukhi, Y. Huang, A.T. To, T. Sooknoi, D.E. Resasco, *J. Catal.* 290 (2012) 90.